Complete Characterization of Ultrashort Pulse Sources at 1550 nm

John M. Dudley, Liam P. Barry, *Member, IEEE*, John D. Harvey, *Member, IEEE*, Mark D. Thomson, Benn C. Thomsen, Paul G. Bollond, *Member, IEEE*, and Rainer Leonhardt

(Invited Paper)

Abstract— **This paper reviews the use of frequency-resolved optical gating (FROG) to characterize mode-locked lasers producing ultrashort pulses suitable for high-capacity optical communications systems at wavelengths around 1550 nm. Second-harmonic generation (SHG) FROG is used to characterize pulses from a passively mode-locked erbium-doped fiber laser, and both single-mode and dual-mode gain-switched semiconductor lasers. The compression of gain-switched pulses in dispersion compensating fiber is also studied using SHG-FROG, allowing optimal compression conditions to be determined without *a priori* assumptions about pulse characteristics. We also describe a fiber-based FROG geometry exploiting cross-phase modulation and show that it is ideally suited to pulse characterization at optical communications wavelengths. This technique has been used to characterize picosecond pulses with energy as low as 24 pJ, giving results in excellent agreement with SHG-FROG characterization, and without any temporal ambiguity in the retrieved pulse.**

Index Terms— **Nonlinear optics, optical fiber lasers, optical fibers, optical pulse compression, optical pulse generation, optical pulse measurements, semiconductor lasers, ultrafast optics.**

I. INTRODUCTION

A S THE demand for high-capacity optical communications systems continues to grow, there will be an increasing need to develop ultrashort pulse sources at wavelengths around 1550 nm corresponding to the low-loss window of silica-based optical fibers. The characterization of ultrashort pulses at this wavelength is therefore extremely important for optical communications applications [1]. The technique of frequency-resolved optical gating (FROG) is now well established as a reliable and accurate technique for ultrashort pulse characterization [2] and has been extensively applied to a variety of mode-locked laser sources [3]–[5]. This technique has also assisted in the development of sub-10-fs lasers [6]. Although the complete pulse characterization afforded by the FROG technique clearly has many applications in optics, until recently, its use in optical communications research has been

limited. It has, however, been used to study a variety of pulse evolution effects in optical fibers around 1550 nm, including pulse compression and broadening from propagation in the anomalous and normal dispersion regimes, respectively [7], four-wave mixing about the fiber zero-dispersion wavelength [8], and the evolution of a high-order soliton over half a soliton period [9]. In addition, FROG has been applied to the measurement of nonlinear and dispersive properties of fibers [10].

In this paper, we review a series of experiments which have extended the use of FROG in optical communications research by applying it to study laser sources producing pulses typical of those required for high-capacity networks. In Section II, we report the characterization of three different sources of picosecond pulses around 1550 nm: a figure-of-eight erbium-doped fiber laser [11], a single-mode gain-switched InGaAsP semiconductor laser [12], and a dual-mode gain-switched InGaAsP semiconductor laser [13]. We also describe experiments studying pulse compression in dispersion-compensating fiber. In Section III, we discuss pulse characterization around 1550 nm using a novel new *Fiber-FROG* geometry based on a third-order nonlinear process in optical fibers. We discuss several issues relating to the practical implementation of Fiber-FROG and show that, for picosecond pulses around 1550 nm, it provides a sensitivity comparable to second-harmonic generation (SHG) FROG, but without any direction-of-time ambiguity in the retrieved pulse.

II. SOURCE CHARACTERIZATION AT 1550 nm USING SHG FROG

In these experiments, a standard SHG FROG setup as described in [2] was used, based on the spectral resolution of the output from a noncollinear autocorrelator. SHG was performed in a BBO crystal with an interaction length ≈ 250 μm. With this interaction length, the expected sinc^2 variation in the SHG response [14] was negligible over a 100-nm bandwidth about 1550 nm. The SHG output was spectrally resolved using a grating spectrometer with a 1024-element cooled photodiode array mounted on the output. The spectral resolution was $\Delta\lambda = 0.03$ nm. The autocorrelator delay was controlled by a stepping motor with temporal resolution of $\Delta\tau = 6.7$ fs. The intrinsic direction-of-time ambiguity present in the retrieved pulse from SHG FROG was removed by an additional FROG measurement after propagation through a short length of fiber
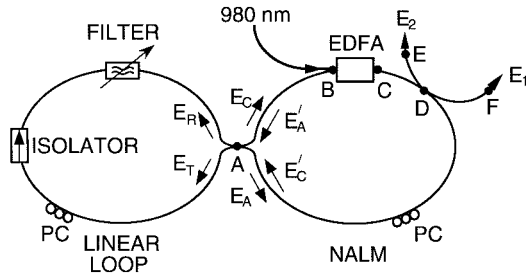
Fig. 1. Schematic diagram of F8L showing notation for intracavity and output fields. The NALM fiber lengths are: AB = 2.4 m, BC = 5.5 m, CD = 2.0 m, DA = 27.4 m, DE = 2.5 m, DF = 4.6 m. A 50:50 coupler was used at point A and a 70:30 coupler at point D.

of known dispersion. Pulse retrieval routinely gave retrieval errors of $G < 0.005$ on a 128×128 grid [2]. In addition, for all the experimental results reported below, the standard checks on the quality of the data were made [2], including inspection of the FROG frequency and delay marginals, and comparing the spectrum and autocorrelation derived from the retrieved field with those directly measured.

A. Passively Mode-Locked Figure-of-Eight Erbium-Doped Fiber Laser

Since they were first developed in the 1980s, erbium-doped fiber lasers (EDFL's) have been the subject of much research [15], [16]. Since the erbium gain band is around 1550 nm, there has been particular interest in their applications in optical communications. Mode-locked EDFL's have been widely used in ultrafast optics [17], and as ultrashort pulse sources in high-capacity network experiments [18]. There are many configurations for EDFL mode locking [15]–[17], and Fig. 1 shows one popular configuration known as the figure-of-eight laser (F8L) [19]. The F8L cavity consists of a nonlinear amplifying loop mirror (NALM) coupled via a 50:50 coupler to a linear fiber loop containing an optical isolator to ensure unidirectional propagation. The NALM consists of a fiber Sagnac interferometer with an asymmetrically placed gain segment provided by an erbium-doped fiber amplifier (EDFA) [20]. Counterpropagating pulses in the NALM develop a differential nonlinear phase shift due to the asymmetric placement of the EDFA, and a differential linear phase shift (the so-called "phase bias") from the intrinsic loop birefringence and a polarization controller (PC) [21]. With correct adjustment of the phase bias, the NALM acts as a nonlinear ultrafast optical switch, transmitting high-intensity pulses and reflecting low intensity pulses [22]. The combination of the NALM and the optical isolator acts as an effective saturable absorber for passive modelocking. For our F8L shown in Fig. 1, the linear loop also contained a spectral filter (FWHM ≈2 nm) for wavelength tunability. The linear loop had a total length of 12.6 m, and the NALM a total length of 37.3 m. The lengths of the individual NALM segments are listed in the figure caption. The NALM output coupler had a transmission of 70%. With the exception of the EDFA, all fiber was standard telecommunications-grade single-mode fiber (SMF) (Corning SMF-28).
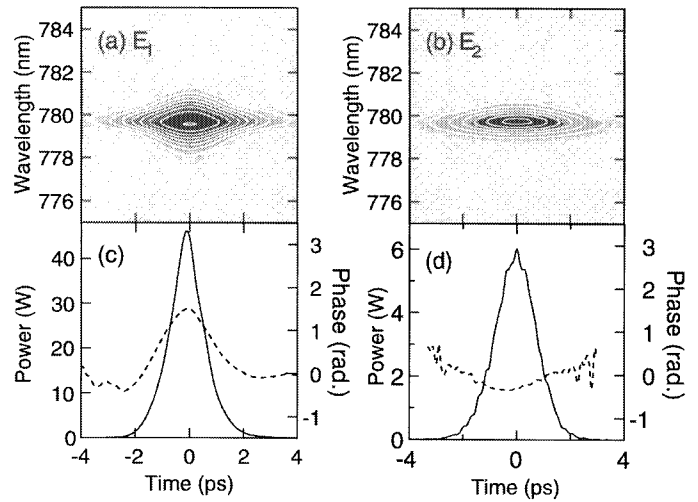

Fig. 2. (a), (b) SHG FROG traces and (c), (d) retrieved intensity (solid line, left axis) and phase (dashed line, right axis) for pulses E_1 and E_2 as indicated.

The operation of the NALM in determining the steady-state operation of the F8L has been investigated theoretically [20], but experimental studies to confirm the theoretical results have been limited [22] because of incomplete knowledge of the intracavity pulse evolution. In our experiments, this intracavity evolution has been experimentally determined by exploiting the complete pulse characterization provided by FROG. By characterizing pulses coupled out of the NALM in both the clockwise and counterclockwise directions, the intracavity fields in the NALM can be determined using numerical propagation, allowing the switching mechanism to be fully characterized. At a wavelength of 1559 nm, stable single-pulse operation at a 4.1-MHz repetition rate was achieved at a pump power of 10 mW. Fig. 2(a) and (b) shows the measured SHG FROG traces of the clockwise and counterclockwise output pulses E_1 and E_2, respectively. The corresponding retrieved pulses are shown in Fig. 2(c) and (d), respectively, with the arbitrary intensity obtained from the pulse retrieval algorithm scaled to show the instantaneous power in watts. The clockwise output E_1 is taken immediately after the EDFA, with peak power and FWHM of 46 W and 1.34 ps, respectively. Its phase shift is consistent with positive chirp acquired from the effects of self-phase modulation (SPM) and normal dispersion in the EDFA. The counterclockwise output E_2 has peak power and FWHM of 6 W and 1.70 ps, respectively, with its lower peak power arising since it is coupled out of the NALM before amplification in the EDFA. Its propagation within the 27.4-m phase-shifting length of the NALM is therefore governed primarily by anomalous dispersion in SMF, and Fig. 2(d) clearly shows the expected negative quadratic phase.

With complete characterization of the output fields, the intracavity fields were determined using a numerical model of pulse propagation in the output coupler and in the different segments of the NALM. Our F8L design was similar to that described in [22], where it was shown that, with nonpolarization preserving fiber, nonlinear polarization evolution is negligible, and the pulses propagating within the laser experience only scalar nonlinear phase shifts. This greatly simplifies the study
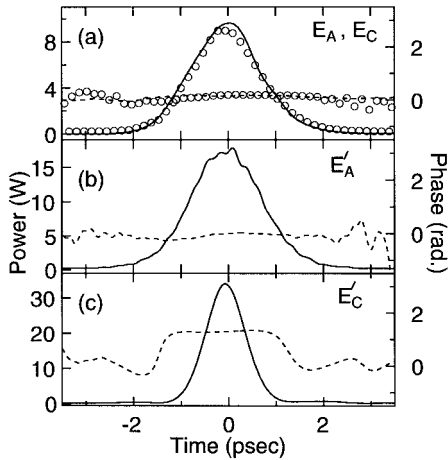
Fig. 3. (a) Intensity (solid line, left axis) and phase (dashed line, right axis) of back-propagated pulse E_A compared with the results for pulse E_C (open circles). (b), (c) Intensity and phase of clockwise E_C' and counterclockwise E_A' pulses incident on the 50:50 coupler.
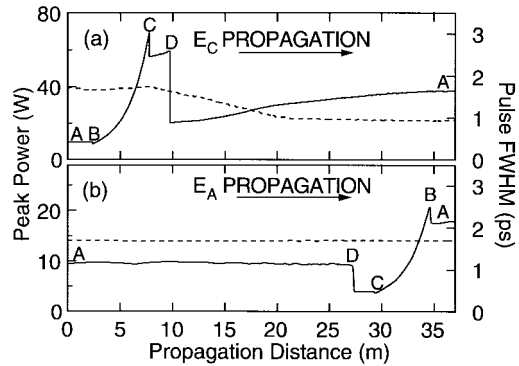

Fig. 4. Intracavity propagation within the NALM in (a) the clockwise and (b) the counterclockwise directions. In each case, the solid line (left axis) shows the evolution of the pulse peak power, whilst the dashed line (right axis) shows the evolution of the pulse FWHM. The discontinuities are associated with coupling losses at points B and C, and output coupling at point D.

of the F8L operation, allowing pulse propagation in each fiber segment to be modeled using a scalar nonlinear Schrödinger equation [23]

$$\frac{\partial A}{\partial z} = -\frac{i\beta_2}{2}\frac{\partial^2 A}{\partial T^2} + i\gamma|A|^2 A + \frac{1}{2}g \qquad (1)$$

where $A(z, T)$ is the electric field envelope in a comoving frame, γ and β_2 are the nonlinearity and group velocity dispersion parameters, respectively, and g accounts for isotropic attenuation or gain. The parameters of SMF are well known, so the backward propagation of output E_2 accurately determines the counterclockwise field E_A leaving the 50:50 coupler. For SMF propagation, attenuation was neglected and we used $\gamma = 1.2 \times 10^{-3}$ W^{-1}·m^{-1} and $\beta_2 = -23$ ps^2/km [10]. The solid and dashed lines in Fig. 3(a) show, respectively, the intensity and phase of this back-propagated field E_A. To study the complete intracavity evolution of pulses in the NALM, propagation within the EDFA must be modeled, but the EDFA dispersion and nonlinearity parameters are not known as accurately as for SMF. However, since the fields E_A and E_C which leave the 50:50 coupler are necessarily identical (within a constant phase shift of $\pi/2$ due to the coupler), the EDFA parameters can be determined by a fitting procedure. This is achieved by backward-propagating the clockwise output E_1 to obtain an estimate for field E_C for some initial choice of EDFA parameters, and using a numerical algorithm to determine the optimum EDFA parameters to minimize the error between this back-propagated field and the field E_A. For a measured EDFA gain $g = 0.45$ m^{-1}, this procedure yielded EDFA parameters of $\beta_2 = +48$ ps^2/km and $\gamma = 6.0 \times 10^{-3}$ W^{-1}·m^{-1}, in good agreement with measurements of similar erbium-doped fiber [24]. The open circles in Fig. 3(a) show the intensity and phase of the optimized field E_C, showing good agreement with the field E_A. Note that the $\pi/2$ difference between the phases of E_A and E_C is not shown. Significantly, it is clear from these results that E_A and E_C have a very small phase variation (<0.1 rad) over the pulse FWHM. Using values for peak power and FWHM of 9.5 W and 1.70 ps, respectively, the soliton order of the pulses E_A and E_C is calculated to

be $N \approx 0.7$. The 50% loss at coupler implies that the pulse incident on the coupler from the linear loop of the F8L is thus close to a fundamental soliton, consistent with the observation that there is no significant phase variation across the pulses.

The pulse evolution in the NALM is determined by the forward-propagation of the fields E_A and E_C. Fig. 4(a) and (b) shows the evolution of the peak power (solid line) and FWHM (dashed line) of E_A and E_C respectively as they propagate in the NALM, clearly showing the difference between counterclockwise and clockwise propagation. The intensity and phase of the pulses E_A' and E_C' incident on the 50:50 coupler after propagation in the NALM are shown in Fig. 3(b) and (c), respectively. The incident counterclockwise field E_A' in Fig. 3(b) has peak power and FWHM of 17.6 W and 1.70 ps, with a small phase variation of 0.2 rad across the pulse FWHM. There is little difference between the intensity and phase characteristics of E_A' and E_A since most of the counterclockwise propagation in the NALM is at low power. By contrast, most of the clockwise propagation in the NALM is at high power, and the clockwise field E_C' in Fig. 3(c) clearly shows the effect of pulse compression and nonlinear phase distortion. Its peak power and FWHM are 38 W and 0.94 ps, respectively, and low-intensity wings can be seen on the pulse. We note, however, that although there is a phase shift of around 1.3 rad between the peak of the pulse and the wings, there is less than 0.1-rad variation in the phase across the pulse FWHM.

The switching of the NALM occurs when pulses E_A' and E_C' recombine in the central 50:50 coupler. The switching efficiency depends on both the intensity and phase characteristics of these pulses, and the absolute differential phase shift developed during propagation in the NALM. The transmission of an ideal NALM with a 50:50 central coupler can be written in the general form $T = 0.5(1 - \cos[\Delta\phi_{NL} + \Delta\phi_B])$ where $\Delta\phi_{NL}$ and $\Delta\phi_B$ are the differential nonlinear phase shift and the phase bias, respectively [22]. For an ideal NALM, optimum switching, therefore, occurs when the total differential phase shift $\Delta\phi_T = \Delta\phi_{NL} + \Delta\phi_B = \pi$. The switching characteristics of the NALM during steady-state operation of the F8L were investigated by numerically interfering E_A' and E_C' as a function of total differential phase shift. The resultant calculated switch-
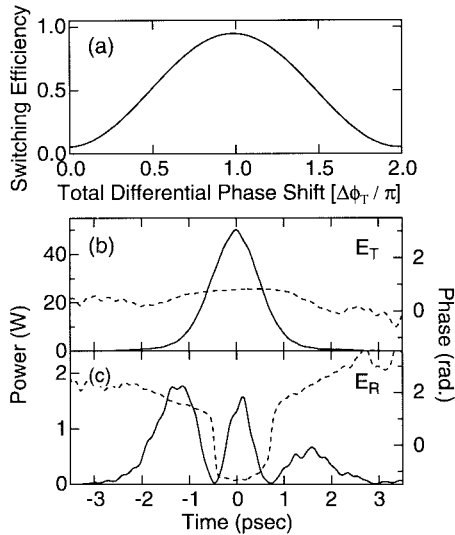
Fig. 5. (a) Calculated switching efficiency as a function of total differential phase shift in the NALM. For optimum switching, (b), (c) show the corresponding transmitted and reflected pulses E_T and E_R, respectively.

Fig. 6. Schematic diagram of SSGS laser configuration.

ing efficiency is shown in Fig. 5(a). As expected, optimum switching of 95% is obtained with $\Delta\phi_T = \pi$. The transmitted and reflected fields E_T and E_R can be conveniently calculated and are shown in Fig. 5(b) and (c), respectively, for the case of optimum switching. Significantly, when the calculated transmitted field E_T is propagated through the linear loop, the field incident on the NALM is consistent with fields E_A and E_C obtained from the back-propagation of the experimental fields, indicating that the stable regime of F8L operation in our experiments coincided with optimum switching efficiency. We note that, while all of these features are consistent with theoretical models of F8L operation, the experimental FROG characterization has provided additional physical insight and revealed some additional interesting features. Notably, these experiments have shown that the switching in the NALM occurs as the result of the interference between two pulses (E'_A and E'_C) of significantly different duration. Although this leads to a complex reflected pulse (E_R) at the coupler, efficient switching is still possible because of the uniform phase shifts developed across pulses E'_A and E'_C in the NALM.

B. Single-Mode Gain-Switched InGaAsP Fabry–Perot Laser Diode

Semiconductor sources of ultrashort pulses around 1550 nm have naturally attracted much attention because of their compactness, ease of fabrication, and their ability to be integrated with other devices such as modulators and amplifiers. One very convenient method to generate ultrashort pulses from semiconductor lasers involves the direct high-frequency modulation of the laser driving current in a process known as gain-switching [25]. This is particularly attractive since the repetition rate of the pulse train can be continuously varied by simply adjusting the gain-switching frequency. For high-capacity network applications, single-longitudinal mode operation is also desirable, usually achieved via distributed feedback (DFB) from a grating integrated within the laser
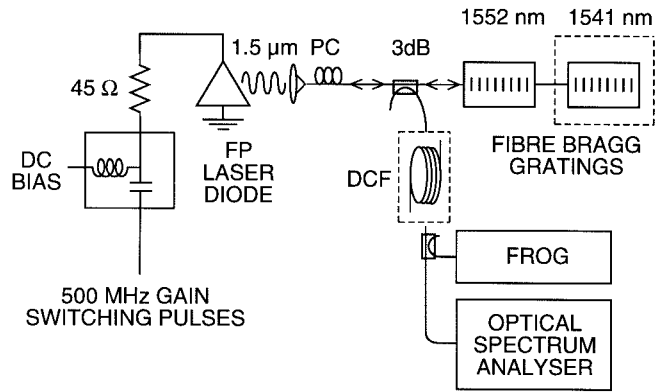
diode structure. An alternative approach which has recently received much attention is the self-seeding of inexpensive Fabry–Perot (FP) laser diodes, and experiments have reported a wide range of self-seeded gain-switched (SSGS) configurations [26]–[31]. With self-seeding, an external cavity containing a wavelength-selective element reinjects a small fraction of the output light back into the gain-switched laser at only one longitudinal mode frequency. Provided that reinjection occurs during the pulse build-up time in the FP laser, gain is suppressed in all but the reinjected mode, and the laser produces a stable train of single-mode pulses. This SSGS technique is advantageous when compared to DFB lasers since it allows convenient wavelength-tunable output with low pulse-to-pulse timing jitter [28]. Recent experiments have also demonstrated multiwavelength output suitable for application in wavelength division multiplexing (WDM) systems [30].

An intrinsic problem associated with gain-switching is the presence of a large frequency chirp across the pulses which arises due to the variation in carrier density (and hence refractive index) in the gain region during the injection of the electrical gain-switching pulse [29]. This chirp is also present in the SSGS configuration. For practical applications of gain-switched pulses, chirp compensation is usually employed, using dispersion-compensating fiber (DCF) [29], [32]–[34] or chirped fiber Bragg gratings [35]. In the experiments to date, however, the conditions for optimum compression have been obtained using an approximate pulse compression model assuming linearly chirped Gaussian pulses [29], [32], [33] or by trial and error using various lengths of DCF [34]. With FROG, however, the direct intensity and phase characterization of the SSGS laser pulses obviates the need for an approximate model of pulse compression, and the optimum compression conditions can be determined with no *a priori* assumptions about the pulse intensity distribution or chirp characteristics.

Fig. 6 shows our experimental setup. The FP laser was a temperature-controlled 1.5-μm InGaAsP device, with a longitudinal mode spacing of 1.1 nm, a threshold current of 27 mA, and a modulation bandwidth of 10 GHz. With the laser biased below threshold at 5 mA, gain-switching was carried out around 500 MHz using electrical pulses of 13-V amplitude and 80-ps FWHM [27]. Gain-switching without external cavity reinjection generated 12-ps pulses (FWHM) with a multimode
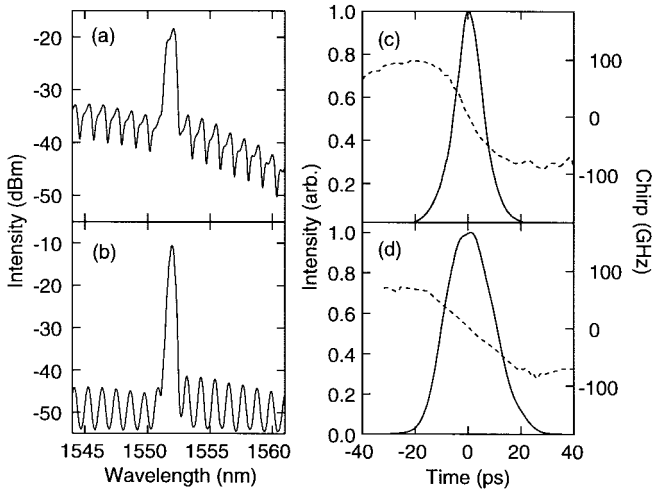
Fig. 7. Spectra for SSGS operation with SMSR's of (a) 15 dB and (b) 30 dB. Also shown is the corresponding (c) retrieved intensity (solid line, left axis) and (d) chirp (dashed line, right axis).
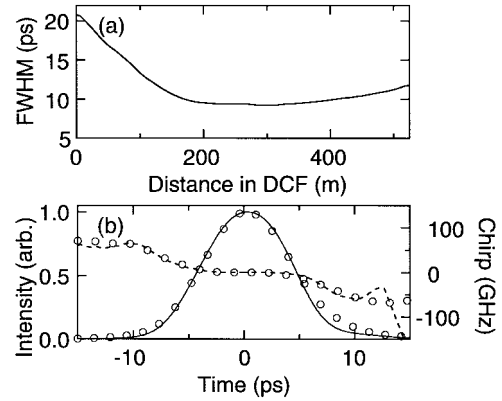

Fig. 8. (a) Simulated evolution in DCF for the pulse in Fig. 7(d). The intensity and chirp of (b) the optimally compressed pulse after 300 m are shown as the solid and dashed lines, respectively, and compared with experimental results (circles).

spectrum. We used either one or two fiber Bragg gratings in the external cavity for single-mode or dual-mode operation. In this section, we consider only single-mode operation using a single grating with central reflection wavelength of 1552 nm and bandwidth of 0.3 nm. The external cavity also contained a polarization controller (PC) and a 3-dB coupler. SSGS operation required temperature adjustment of the laser so that an oscillating longitudinal laser mode coincided with the central reflection wavelength of the grating, and tuning of the gain-switching frequency to 496.76 MHz, corresponding to the 26th external-cavity harmonic. The fraction of external-cavity reinjection was controlled by varying the polarization of the reflected signal using the PC.

The laser output was characterized using SHG FROG as well as measurements of the optical spectrum and autocorrelation. With varying reinjection level, the side-mode supression ratio (SMSR) between the lasing mode and adjacent modes was observed to vary significantly, and stable laser operation was observed for SMSR values from 15 to 35 dB (corresponding to estimated reinjection levels of 0.1%–6%). Higher reinjection levels resulted in instabilities [36]. Fig. 7(a) and (b) shows the measured spectra for SMSR's of 15 dB and 30 dB, and Fig. 7(c) and (d) shows the pulse characteristics retrieved from the measured SHG FROG traces. Within experimental error, the average output power was measured at around 0.17 mW for all SMSR values, and, to obtain good signal-to-noise ratio (SNR) in the FROG measurements, an erbium-doped fiber amplifier amplified the SSGS pulses to a peak power of around 1 W. For the pulse durations and power levels considered here, this amplification introduced negligible intensity or phase distortion. Note that for these results we directly plot the pulse chirp in gigahertz, obtained from the retrieved phase $\phi(t)$ using $\delta\nu(t) = -(2\pi)^{-1}d\phi(t)/dt$. These results show that greater reinjection results in improved SMSR and improved spectral symmetry, arising due to the reduction in the peak inversion reached during the pulse emission process in the presence of the reinjected signal [37]. Significantly, the FROG characterization also reveals that these

improved spectral characteristics are associated with a smaller nonlinear chirp component on the pulse, as is clear from a comparison of Fig. 7(c) and (d). This result implies that SSGS operation at high injection levels should produce linearly chirped pulses suitable for the generation of near-transform-limited pulses after compression in DCF.

To test this quantitatively, we numerically simulated the propagation of the linearly chirped pulse shown in Fig. 7(d) in DCF. These simulations were based on the standard NLSE, assuming a normal dispersion of $D = -102$ ps/nm $\cdot$ km (corresponding to Lucent DK-SM fiber) and neglecting nonlinear effects at the peak power levels in our experiments. The expected evolution of the pulse FWHM as a function of propagation distance is shown in Fig. 8(a) and indicates optimum compression after 280–320 m. The intensity and phase of the expected optimally compressed pulse are shown as the solid and dashed lines in Fig. 8(b). These simulations were tested experimentally using 300 m of Lucent DK-SM DCF, and the intensity and chirp characteristics retrieved from the measured FROG trace are shown as the open circles in Fig. 8(b). There is clearly good agreement between experiment and simulation, and the chirp compensation across the center of the pulse is clearly shown. The time–bandwidth product after compression is $\Delta\tau\Delta\nu \approx 0.5$, with a lower value not obtained because of residual nonlinear chirp in the input pulses. These results indicate that the numerical propagation of the pulse retrieved from a measured FROG trace accurately determines the optimum conditions for compression, and we expect that this approach will find wide application, greatly simplifying experimental procedures for accurate chirp compensation.

C. Dual-Mode Gain-Switched InGaAsP FP Laser Diode

As discussed above, a second fiber Bragg grating could be used to provide feedback at a second longitudinal mode frequency resulting in dual-mode operation. The dual-mode operation of semiconductor lasers is a topic of much current interest, since the resulting laser output has a high frequency intensity modulation in the gigahertz–terahertz frequency range, suitable for applications in millimeter-wave optical communication systems and in terahertz difference
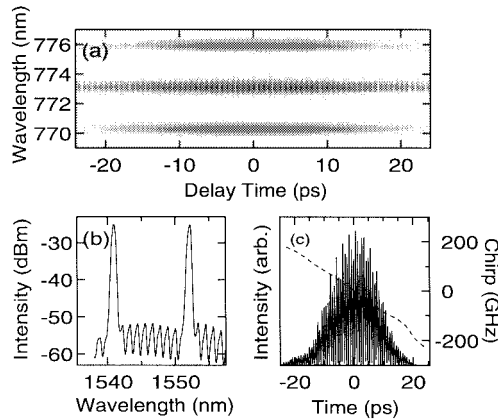
Fig. 9. (a) SHG FROG trace for dual-mode SSGS operation. (b) Corresponding dual-mode spectrum. (c) Retrieved intensity (solid line, left axis) and chirp (dashed line, right axis).

frequency generation [38], [39]. In our experiments feedback was provided from fiber Bragg gratings at 1552 nm and 1541 nm. As with single-mode operation, it was necessary to carefully control the FP laser temperature control and to choose appropriate external cavity fiber lengths so that the feedback from the gratings arrived back at the laser during the build-up of an optical pulse in the gain-switching cycle.

The measured SHG FROG trace of the dual-mode laser is shown in Fig. 9(a). It is clear that the FROG trace shows appreciable signal at the two SHG wavelengths corresponding to each individual oscillating mode, but it also clearly shows a temporally modulated signal at a wavelength corresponding to intermodal sum frequency mixing. Fig. 9(b) shows the corresponding spectrum (SMSR = 25 dB) and Fig. 9(c) the corresponding oscillatory structure in the retrieved field intensity. The retrieved intensity shows near 100% intensity modulation at 1.4 THz, corresponding to the beating between the two longitudinal modes separated by 11.2 nm. This oscillation is associated with π phase discontinuities on the phase obtained from the FROG phase retrieval algorithm, but these are conveniently removed to determine the residual phase variation and chirp, and this is also shown in Fig. 9(c).

III. COMPLETE PULSE CHARACTERIZATION USING FIBER-FROG

The results above have clearly shown that FROG has important applications for ultrashort pulse source characterization around 1550 nm. In these experiments, SHG FROG was used because of the picojoule pulse energies involved, but an additional propagation experiment (or *a priori* knowledge of the sign of the pulse chirp) was required with each measurement to remove the direction-of-time ambiguity in the retrieved pulse. FROG geometries using third-order nonlinear processes [2] do not possess this ambiguity, but require incident pulse energies of nanojoules or greater. These existing geometries, however, are all based on nonlinear effects in bulk materials, with the nonlinear interaction length limited by effects such as phase matching, dispersion, and geometrical beam divergence. In this section, we describe the use of the third-order process of cross-phase modulation (XPM) in an optical fiber to allow complete
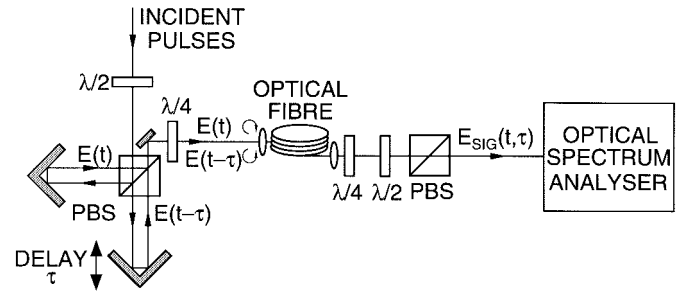

Fig. 10. Experimental setup for Fiber-FROG.

pulse characterization via a *Fiber-FROG* geometry. Although the use of XPM in bulk media has been previously used for complete pulse characterization of millijoule energy pulses [40], [41], we describe how suitable experimental parameters can be chosen to minimize the effects of dispersion and allow a large interaction length in fiber to be used to yield picojoule sensitivity comparable to SHG FROG, but with no direction-of-time ambiguity.

In general, pulse propagation in optical fibers depends on both dispersive and nonlinear effects. However, depending on the incident pulse characteristics and the particular fiber used, pulses can propagate such that nonlinear effects dominate and dispersion is negligible [23]. In this case, the nonlinear pulse evolution in the fiber can be exploited for use in a Fiber-FROG geometry, as shown in Fig. 10. Incident pulses are split into two replicas with orthogonal linear polarizations (LP's) using a polarizing beamsplitter (PBS) before being recombined with a variable delay. A half-wave plate ($\lambda/2$) at the input ensures that the output reference pulse $E(t)$ and the delayed replica $E(t - \tau)$ have equal amplitudes. A quarter-wave plate ($\lambda/4$) converts these LP-fields into counterrotating circular-polarized (CP) fields which are coupled into a length of fiber, where each pulse experiences a nonlinear phase shift due to the effects of SPM and XPM from the copropagating pulse with the opposite CP state. Note that the use of CP waves in this way increases the effect of XPM by a factor of two relative to LP fields and allows residual linear fiber birefringence to be neglected. A $\lambda/4$ plate at the fiber output converts these CP fields back into orthogonal LP fields, one of which is selected with a $\lambda/2$ plate and PBS to generate an output signal $E_{\mathrm{SIG}}(t,\tau)$ [23]

$$E_{\mathrm{SIG}}(t,\tau) = E(t)\exp\left[i\gamma L\left(\frac{2}{3}|E(t)|^2 + \frac{4}{3}|E(t-\tau)|^2\right)\right]. \quad (2)$$

Here γ is the fiber Kerr nonlinearity coefficient and L is the fiber length. In the frequency domain, the spectral resolution of $E_{\mathrm{SIG}}(t,\tau)$ yields a spectrum which contains a constant amount of spectral broadening due to SPM and a delay-dependent nonlinear frequency shift (or a phase gate) due to XPM. Explicitly, the corresponding Fiber-FROG trace is given as

$$I_{\mathrm{SIG}}(\omega,\tau) = \left|\int E(t)\exp\left[i\gamma L\left(\frac{2}{3}|E(t)|^2 + \frac{4}{3}|E(t-\tau)|^2\right)\right]\right.$$
$$\left. \cdot \exp(i\omega t)\,dt\right|^2. \quad (3)$$

With Fiber-FROG, we have used the standard FROG algorithm of generalized projections (GP's) [2] to carry out phase retrieval, although we note that phase retrieval can be carried out using alternative algorithms. One particularly simple algorithm described in [40] is known as the "ENSTA" algorithm. With ENSTA, phase retrieval involves sequentially cycling though each of the spectra measured at different delays and applying an inverse propagation operation at each step to obtain a successively better estimate for the original field. The phase retrieval in GP is significantly different, since all the measured spectra are used simultaneously. Although this makes it more complex, we have found that GP is superior to ENSTA in its resistance to noise and its ability to retrieve severely distorted pulses. In particular, we have found that, for nonlinearly chirped pulses, ENSTA stagnates if the magnitude of the nonlinear phase shift on the input pulse exceeds that developed on the pulse due to XPM. Using GP, however, we have found that stagnation does not occur under these conditions and successful pulse retrieval is possible. An additional feature of GP is that it is not necessary to know the value of the nonlinearity coefficient γ accurately, since this can be included as a free parameter in the algorithm. This can be advantageous, since there can be significant variation in γ for different fibers. The standard GP algorithm does require some modification for Fiber-FROG since the XPM phase gating depends on the absolute pulse peak power in the fiber, and arbitrary normalization of the Fiber-FROG trace is not possible. In our algorithm, the Fiber-FROG trace is normalized such that the measured spectrum for each value of delay contains the same (experimentally determined) energy.

We now discuss some practical issues. Since Fiber-FROG is based on phase gating, there are no geometrical phase-matching requirements to be met, and the trace is centered on the pulse's fundamental wavelength. These features simplify the experimental setup. In addition, the use of an optical waveguide reduces sensitivity to environmental noise. The most important factor in Fiber-FROG is the choice and length of optical fiber. In particular, the length must be short enough so that dispersion is negligible, yet long enough so that the frequency shift due to XPM is measurable. These constraints depend both on the properties of the incident pulses as well as the particular fiber used, but we have obtained some guidelines using numerical simulations for a variety of incident test pulses and using noise levels typical of experimental conditions [42]. A more complete discussion of these issues will be given elsewhere [43], but the important results can be summarized. Consider a pulse with peak power P_0 and rms duration T_0 in a fiber of length L with nonlinearity coefficient γ and group-velocity dispersion (GVD) and third-order dispersion (TOD) parameters β_2 and β_3, respectively. Successful retrieval in Fiber-FROG then requires that $P_0 \geq 0.1/\gamma L$, with the minimum measurable pulse duration given by $T_0 \geq (20|\beta_2|L)^{1/2}$ if GVD dominates, or $T_0 \geq (20|\beta_3|L)^{1/3}$ if TOD dominates. These constraints can be conveniently used for experimental design given knowledge of the nonlinear and dispersive properties of particular fiber. For example, with practical lengths ($\gtrsim$cm) of standard silica fiber with incident pulses of nanojoule energy, sub-100-fs pulse char-
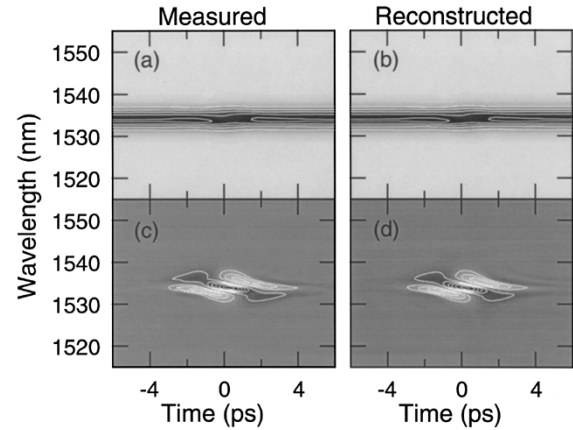

Fig. 11. (a) Measured and (b) reconstructed Fiber-FROG traces for F8L pulses. (c), (d) Corresponding background-free results.

acterization is possible at all near-infrared wavelengths above 1000 nm.

Fiber-FROG is most useful at wavelengths where the intrinsic fiber dispersion is minimized, making it ideally suited for pulse characterization at the communications wavelengths of around 1310 nm in standard silica fiber, or around 1550 nm in DSF. In our experiments, we have used it to characterize pulses from the F8L described above operating at a wavelength of 1534 nm. For a nonlinear medium, we used a commercial 20-m patch-cord of DSF (Corning SMF-DS) with $\beta_2 = 9.5 \times 10^{-4}$ ps^2/m, $\beta_3 = 1.17 \times 10^{-4}$ ps^3/m, and $\gamma = 1.8 \times 10^{-3}$ W^{-1}·m^{-1} at 1534 nm. For these parameters, the minimum required peak power P_0 is 4 W, corresponding to a minimum incident peak power of 12 W in our setup, once experimental losses are also considered. Measurements of the pulses were made directly from the laser and also after external pulse compression. To provide an accurate test of Fiber-FROG, the results were compared with standard SHG FROG characterization in each case.

Fig. 11(a) shows the measured Fiber-FROG trace for the F8L pulses, and Fig. 11(b) shows the reconsructed trace after phase retrieval using the GP algorithm. The measured SHG FROG trace is not shown, but was similar to that shown in Fig. 2(a). In contrast to SHG FROG, the Fiber-FROG trace is centered about the fundamental wavelength and contains spectral information for all values of delay. Far from zero delay, the spectrum in the Fiber-FROG trace is simply that of the input pulse after propagation through the DSF. Near zero-delay, however, XPM causes a delay-dependent nonlinear frequency shift. This can be more clearly seen by the subtraction of the constant spectrum for large delay to yield corresponding "background-free" traces, as shown in Fig. 11(c) and (d). Fig. 12 shows additional results after the F8L pulses were amplified to a peak power of 100 W and propagated through 20 m of SMF-28 in the anomalous dispersion regime. In this case, the interaction of nonlinear and dispersive effects results in significant spectral and temporal distortion, and Fig. 12 shows how this leads to a more complex measured Fiber-FROG trace. With the data in Figs. 11 and 12, excellent pulse retrieval using GP was achieved as is clear from a visual comparison of the measured and reconstructed traces.
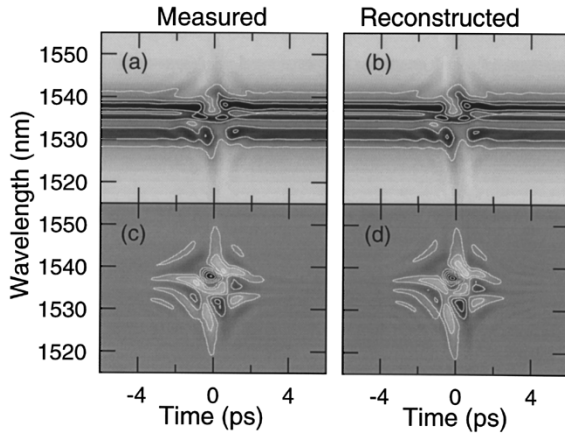
Fig. 12.   (a) Measured and (b) reconstructed Fiber-FROG traces for compressed F8L pulses. (c), (d) Corresponding background-free results.
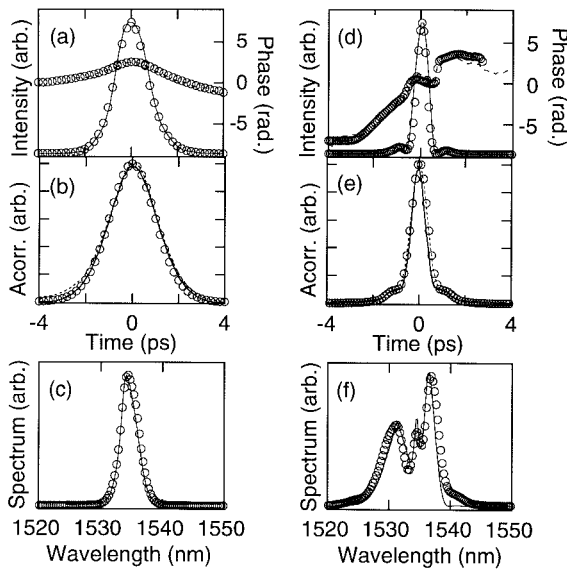

Fig. 13.   F8L pulse characteristics showing (a) intensity (solid line, left axis) and phase (dashed line, right axis), compared with SHG FROG results (circles). (b) Measured autocorrelation (solid) obtained from the delay marginal (dashed) and from the retrieved pulse (circles). (c) Measured spectrum (solid) and that derived from the retrieved pulse (circles). (d)–(f) Equivalent results for the pulses after compression.

Fig. 13(a)–(c) and Fig. 13(d)–(e) present the retrieved pulse data for the results in Figs. 11 and 12, respectively. The retrieved intensity and phase are shown in Fig. 13(a) and (d) and compared with the corresponding results from SHG FROG (open circles). It is clear there is very good agreement. We note in particular that, for the unamplified pulses in Fig. 13(a), the intensity FWHM of the retrieved pulses was 1.6 ps and the calculated peak power was 15 W. The corresponding incident pulse energy is 24 pJ. With Fiber-FROG, we have, therefore, achieved a sensitivity usually associated with SHG FROG, but without any direction-of-time ambiguity. The solid lines in Fig. 13(b) and (e) show the measured autocorrelation function, and the solid lines in Fig. 13(c) and (f) show the measured spectrum. As with other FROG geometries, the internal consistency of Fiber-FROG can be checked by calculating marginals from the measured trace and comparing them with independently measured quantities. For Fiber-FROG, the most useful marginal is the delay marginal obtained by calculating

the mean spectral component of the Fiber-FROG trace as a function of delay [40]. This is linearly related to the derivative of the intensity autocorrelation function and can be used to compute the autocorrelation function for comparison with that directly measured. For the results in Figs. 11 and 12, Fig. 13(b) and (e) show this computed autocorrelation function as the dashed line, and it is clear there is good agreement with the measured result. A final check on the data quality is to compare the autocorrelation and spectrum derived from the retrieved pulse with those directly measured. The results in this case are shown as the open circles in Figs. 13(b) and (e) for the autocorrelations and in Figs. 13(c) and (f) for the spectra.

IV. CONCLUSION

Pulse characterization around 1550 nm will become increasingly important as the demand for compact ultrashort pulse sources at this wavelength continues to grow. The results in this paper have demonstrated several applications of the FROG technique to the characterization of pulsed sources at wavelengths around 1550 nm. By measuring the intensity and phase of pulses coupled out of the nonlinear loop of a mode-locked erbium-doped fiber laser, it has been possible to study the steady-state nonlinear switching characteristics and obtain physical insight into the mechanism of passive mode locking in this laser. Similarly, the study of pulses from self-seeded gain-switched semiconductor lasers has revealed that the chirp characteristics vary significantly with external cavity reinjection level, with results indicating in particular that increased reinjection levels are associated with a more linear chirp on the output pulses. Experiments with linearly chirped pulses generated under these conditions have shown how complete pulse characterization using FROG obviates the need for *a priori* assumptions about the pulse characteristics when performing pulse compression. With an SSGS semiconductor laser operating on two longitudinal modes, additional experiments have shown the simultaneous resolution of near-100% terahertz intensity modulation and a residual chirp on the output pulses. We have also used a novel new FROG geometry based on an optical fiber nonlinearity which we expect will find wide application. The technique of Fiber-FROG has been shown to provide accurate pulse characterization at 1550 nm, at sensitivites usually associated with SHG FROG, but without any direction-of-time ambiguity. Significantly, the use of an optical fiber-based nonlinearity lends itself to convenient experimental implementation and allows the possibility of integration with fiber-based equivalents of the bulk-optical elements used in our experiments. We anticipate that this will lead to the development of an all-fiber-based configuration for pulse characterization at communications wavelengths.

REFERENCES

[1] G. P. Agrawal, *Fiber-Optic Communication Systems.* New York: Wiley-Interscience, 1997.
[2] R. Trebino, K. W. DeLong, D. N. Fittinghoff, J. N. Sweetser, M. A. Krumbügel, and B. A. Richman, "Measuring ultrashort laser pulses in

the time-frequency domain using frequency-resolved optical gating," *Rev. Sci. Instrum.*, vol. 68, pp. 3277–3295, 1997.

[3] D. J. Kane, A. J. Taylor, R. Trebino, and K. W. DeLong, "Single-shot measurement of the intensity and phase of femtosecond uv laser pulse using frequency-resolved optical gating," *Opt. Lett.*, vol. 19, pp. 1061–1063, 1994.

[4] B. A. Richman, K. W. DeLong, and R. Trebino, "Temporal characterization of the stanford mid-IR FEL micropulses by FROG," *Nucl. Instrum. Methods Phys. Res. A*, vol. 358, pp. 268–271, 1995.

[5] B. Kohler, V. V. Yakovlev, K. R. Wilson, J. Squier, K. W. DeLong, and R. Trebino, "Phase and intensity characterization of femtosecond pulses from a chirped pulse amplifier by frequency-resolved optical gating," *Opt. Lett.*, vol. 20, pp. 483–485, 1995.

[6] G. Taft, A. Rundquist, M. M. Murnane, I. P. Christov, H. C. Kapteyn, K. W. DeLong, D. N. Fittinghoff, M. A. Krumbügel, J. N. Sweetser, and R. Trebino, "Measurement of 10-fs laser pulses," *IEEE J. Select. Topics Quantum Electron.*, vol. 2, pp. 575–585, 1996.

[7] L. P. Barry, J. M. Dudley, P. G. Bollond, J. D. Harvey, and R. Leonhardt, "Direct characterization of pulse propagation in optical fibers using frequency resolved optical gating," *Electron. Lett.*, vol. 32, pp. 2339–2340, 1996.

[8] J. M. Dudley, L. P. Barry, P. G. Bollond, J. D. Harvey, R. Leonhardt, and P. D. Drummond, "Direct measurement of pulse distortion near the zero-dispersion wavelength in optical fibers using frequency resolved optical gating," *Opt. Lett.*, vol. 22, pp. 457–459, 1997.

[9] J. M. Dudley, L. P. Barry, P. G. Bollond, J. D. Harvey, and R. Leonhardt, "Characterising pulse propagation in optical fibers around 1550 nm using frequency-resolved optical gating," *Opt. Fiber Technol.*, vol. 4, pp. 237–265, 1998.

[10] L. P. Barry, J. M. Dudley, P. G. Bollond, J. D. Harvey, and R. Leonhardt, "Simultaneous measurement of optical fiber nonlinearity and dispersion using frequency-resolved optical gating," *Electron. Lett.*, vol. 33, pp. 707–708, 1997.

[11] P. G. Bollond, L. P. Barry, J. M. Dudley, R. Leonhardt, and J. D. Harvey, "Characterization of nonlinear switching in a fig.-of-eight fiber laser using frequency-resolved optical gating," *IEEE Photon. Technol. Lett.*, vol. 10, pp. 343–345, 1998.

[12] L. P. Barry, B. C. Thomsen, J. M. Dudley, and J. D. Harvey, "Characterization of 1.55 μm pulses from a self-seeded gain-switched Fabry-Perot laser diode using frequency resolved optical gating," *IEEE Photon. Technol. Lett.*, vol. 10, p. 935, 1998.

[13] L. P. Barry, J. M. Dudley, B. C. Thomsen, and J. D. Harvey, "Frequency resolved optical gating measurements of 1.4 THz beat frequencies from a dual-wavelength self-seeded gain-switched laser diode," *Electron. Lett.*, vol. 43, pp. 988–990, 1998.

[14] A. Weiner, "Effect of group velocity mismatch on the measurement of ultrashort optical pulses via second harmonic generation," *IEEE J. Quantum Electron.*, vol. QE-19, pp. 1276–1283, 1983.

[15] L. E. Nelson, D. J. Jones, K. Tamura, H. A. Haus, and E. P. Ippen, "Ultrashort pulse fiber ring lasers," *Appl. Phys. B*, vol. 65, pp. 277–294, 1997.

[16] I. N. Duling III, *Compact Sources of Ultrashort Pulses*. Cambridge, U.K.: Cambridge Univ., 1995.

[17] M. E. Fermann, A. Galvanauskas, G. Sucha, and D. Harter, "Fiber lasers for ultrafast optics," *Appl. Phys. B*, vol. 65, pp. 259–275, 1997.

[18] E. Yoshida, T. Yamamoto, A. Sahara, and M. Nakazawa, "320 Gbit/s TDM transmission over 120 km using 400 fs pulse train," *Electron. Lett.*, vol. 34, pp. 1004–1006, 1998.

[19] I. N. Duling III, "All-fiber ring soliton laser mode-locked with a nonlinear mirror," *Opt. Lett.*, vol. 16, pp. 539–541, 1991.

[20] M. Fermann, F. Haberl, M. Hofer, and H. Hochreiter, "Nonlinear amplifying loop mirror," *Opt. Lett.*, vol. 15, pp. 752–754, 1990.

[21] D. Mortimore, "Fiber loop reflectors," *J. Lightwave Technol.*, vol. 6, pp. 1217–1224, 1988.

[22] A. J. Stentz and R. W. Boyd, "Polarization effects and nonlinear switching in fiber figure-eight lasers," *Opt. Lett.*, vol. 19, pp. 1462–1464, 1994.

[23] G. P. Agrawal, *Nonlinear Fiber Optics*. San Francisco, CA: Academic, 1995.

[24] B. Deutsch and Th. Pfeiffer, "Chromatic dispersion of erbium-doped silica fibers," *Electron. Lett.*, vol. 28, pp. 303–305, 1992.

[25] H. Ito, H. Yokoyama, S. Murata, and H. Inaba, "Picosecond optical pulse generation from an RF modulated AlGaAs laser diode," *Electron. Lett.*, vol. 15, pp. 738–740, 1979.

[26] M. Cavelier, N. Stelmakh, J. M. Xie, L. Chusseau, J. M. Lourtioz, C. Kasmierski, and N. Bouadama, "Picosecond ($<$2.5 ps) wavelength tunable ($\sim$20 nm) semiconductor laser pulses with repetition rates up to 12 GHz," *Electron. Lett.*, vol. 28, pp. 224–226, 1992.

[27] L. P. Barry, R. F. O'Dowd, J. Debeau, and R. Boittin, "Tunable transform limited pulse generation using self-injection locking of a FP laser," *IEEE Photon. Technol. Lett.*, vol. 5, pp. 1132–1134, 1993.

[28] M. Schell, W. Utz, D. Huhse, J. Kassner, and D. Bimberg, "Low jitter single mode pulse generation by a self-seeded, gain-switched Fabry-Perot semiconductor laser," *Appl. Phys. Lett.*, vol. 65, pp. 3045–3047, 1994.

[29] Y. C. Lee and C. Shu, "Wavelength-tunable nearly transform-limited pulses generated by self-injection seeding of a laser diode at an arbitrary repetition rate," *IEEE Photon. Technol. Lett.*, vol. 9, pp. 590–592, 1997.

[30] C. Shu and S. P. Yam, "Effective generation of tunable single- and multiwavelength optical pulses from a Fabry Perot laser diode," *IEEE Photon. Technol. Lett.*, vol. 9, pp. 1214–1216, 1997.

[31] Y. Zhao and C. Shu, "Single-mode operation characteristics of a self-injection seeded Fabry-Perot laser diode with distributed feedback from a fiber grating," *IEEE Photon. Technol. Lett.*, vol. 9, pp. 1436–1438, 1997.

[32] H.-F. Liu, Y. Ogawa, and S. Oshiba, "Generation of an extremely short single-mode pulse ($\sim$2 ps) by fiber compression of a gain-switched pulse from a 1.3 μm distributed-feedback laser diode," *Appl. Phys. Lett.*, vol. 59, pp. 1284–1286, 1991.

[33] K. A. Ahmed, H.-F. Liu, N. Onodera, P. Lee, R. S. Tucker, and Y. Ogawa, "Nearly transform-limited pulse (3.6 ps) generation from gain-switched 1.55 μm distributed feedback laser by using fiber compression technique," *Electron. Lett.*, vol. 29, pp. 54–56, 1993.

[34] L. Chusseau and C. Kasmierski, "Optimum linear pulse compression of a gain switched 1.5 μm DFB laser," *IEEE Photon. Technol. Lett.*, vol. 6, pp. 24–26, 1994.

[35] B. J. Eggleton, P. A. Krug, L. Poladian, K. A. Ahmed, and H. F. Liu, "Experimental demonstration of compression of dispersed optical pulses by reflection from self-chirped optical fiber Bragg gratings," *Opt. Lett.*, vol. 19, pp. 877–879, 1994.

[36] D. S. Seo, H. F. Liu, D. Y. Kim, and D. D. Sampson, "Injection power and wavelength dependence of an external-seeded gain-switched Fabry–Perot laser," *Appl. Phys. Lett.*, vol. 67, pp. 1503–1505, 1997.

[37] Y. Matsui, S. Kutsuzawa, S. Arahira, and Y. Ogawa, "Generation of wavelength tunable gain-switched pulses from FP MQW lasers with external injection seeding," *IEEE Photon. Technol. Lett.*, vol. 9 pp. 1087–1089, 1997.

[38] S. Matsuura, M. Tani, and K. Sakai, "Generation of coherent terahertz radiation by photomixing in dipole photoconductive antennas," *Appl. Phys. Lett.*, vol. 70, 559–561, 1997.

[39] T. Hikada, S. Matsuura, M. Tani, and K. Sakai, "CW terahertz wave generation by photomixing," *Electron. Lett.*, vol. 33, pp. 2039–2040, 1997.

[40] M. A. Franco, H. R. Lange, J.-F. Ripoche, B. S. Prade, and A. Mysyrowicz, "Characterization of ultrashort pulses by cross-phase modulation," *Opt. Commun.*, vol. 140, pp. 331–340, 1997.

[41] H. R. Lange, M. A. Franco, J.-F. Ripoche, B. S. Prade, P. Rousseau, and A. Mysyrowicz, "Reconstruction of the time profile of femtosecond laser pulses through cross-phase modulation," *IEEE J. Select. Topics Quantum Electron.*, vol. 4, pp. 295–300, 1998.

[42] D. N. Fittinghoff, K. W. DeLong, R. Trebino, and C. L. Ladera, "Noise sensitivity in frequency-resolved optical gating measurements of ultrashort pulses," *J. Opt. Soc. Amer. B*, vol. 12, p. 1955, 1995.

[43] M. D. Thomson, J. M. Dudley, L. P. Barry, and J. D. Harvey, "Complete pulse characterization at 1.5 μm using cross-phase modulation in optical fibers," *Opt. Lett.*, vol. 23, pp. 1582–1584, 1998.

John M. Dudley received the B.Sc. and Ph.D. degrees in physics from the University of Auckland, Auckland, New Zealand, in 1987 and 1992, respectively.

In 1992 and 1993, he carried out post-doctoral research studying femtosecond mode-locked lasers and optical parametric oscillators at the University of St. Andrews, Scotland, U.K. In 1994, he took up a lecturing position at the University of Auckland. His current research interests are in the physics of ultrashort pulse generation and measurement, nonlinear optics, and applications in optical communications.

Dr. Dudley is a member of the Optical Society of America, the New Zealand Institute of Physics, the Australian Optical Society, and the Royal Society of New Zealand.

Liam P. Barry (M'98) received the B.E. degree in electronic engineering and the M.Eng.Sc. degree in optical communications from University College Dublin, Ireland, U.K., in 1991 and 1993, respectively, and the Ph.D. degree from the University of Rennes, France, in 1996.

From 1993 to 1996, he was employed as a Research Engineer in the Optical Systems Department of France Telecom's Research Laboratories (CNET), Lannion, France. His doctoral degree was a result of this work. From 1996 to 1998, he worked at the University of Auckland, Auckland, New Zealand, studying optical pulse generation and measurement and the use of optical nonlinearities for high-speed all-optical switching in fiber networks. In March 1998, he took up a lecturing position in the School of Electronic Engineering, Dublin City University, Dublin, Ireland, U.K.

John D. Harvey (M'76) received the B.Sc. and M.Sc. degrees from the University of Auckland, Auckland, New Zealand, in 1965 and 1967, respectively, and the Ph.D. degree from the University of Surrey, U.K., for work in theoretical nuclear physics.

Since 1970, he has worked at the University of Auckland where he now holds a Chair in the Physics Department. In recent years, his research has been concentrated in the areas of nonlinear fiber optics, ultrafast processes, and mode-locked lasers.

Prof. Harvey is a fellow of the New Zealand Institute of Physics and is a member of the Optical Society of America and the Australian Optical Society.

Mark D. Thomson received the B.Tech. degree in optoelectronics and the M.Sc. degree from the University of Auckland, Auckland, New Zealand, in 1997 and 1998, respectively. His M.Sc. research involved studying nonlinear pulse propagation in optical fibers, and the application of fiber non-linearities to ultrashort pulse characaterization. He is currently working toward the Ph.D. degree at the Physikalisches Institut, Johan Wolfang Goethe-Universit, Frankfurt, Germany. His Ph.D. research will study the photophysics of silicon-based materials and terahertz spectroscopy.

Benn C. Thomsen received the B.Tech. degree in optoelectronics and the M.Sc. degree from the University of Auckland, Auckland, New Zealand, in 1997 and 1998, respectively. His M.Sc. research involved studying two-photon absorption in semiconductors and the generation of picosecond pulses from semiconductor lasers. He is currently working toward the Ph.D. degree in physics at the University of Auckland.

Paul G. Bollond (M'93) received the B.Sc., M.Sc., and Ph.D. degrees in physics from the University of Auckland, Auckland, New Zealand, in 1990, 1992, and 1998, respectively. His Ph.D. dissertation was on picosecond pulse generation and propagation in erbium-doped optical fibers.

In 1997, he joined JDS Fitel, Inc., Freehold, NJ, as an Optical Fiber Amplifier Designer in the Lightwave Products Group.

Dr. Bollond is a member the Optical Society of America.

Rainer Leonhardt received the Dipl.Phys. and Dr.rer.nat. degrees from the Technische Universität München, Germany, in 1984 and 1987, respectively.

From 1988 to 1990, he worked at the University of Auckland, Auckland, New Zealand, funded by a Feodor-Lynen research fellowship from the Alexander-von-Humboldt-Stiftung, Germany. In 1991, he took up a lecturing position at the University of Auckland. His current research interests are in the generation of ultrashort pulses, parametric processes in optical fibers, and terahertz spectroscopy.